

Supporting Information

Spectroscopic identification of charge transfer of thiolated molecules on gold nanoparticle via gold nanocluster

Mohammad Tavakkoli Yaraki¹, Noelia Soledad Rubio¹, Anastasiia Tukova¹, Junxian Liu², Yuantong Gu², Liangzhi Kou^{2,*}, Yuling Wang^{1,*}

¹ School of Natural Sciences, Faculty of Science and Engineering, Macquarie University, Sydney, NSW 2109, Australia

²School of Mechanical, Medical and Process Engineering, Queensland University of Technology, Garden Point Campus, Brisbane, Queensland 4001, Australia

*Corresponding authors

A/ Prof. Liangzhi Kou., E-mail: liangzhi.kou@qut.edu.au

Prof. Yuling Wang., E-mail: yuling.wang@mq.edu.

Methods

Chemicals

Hydrogen tetrachloroaurate (III) trihydrate ($\text{HAuCl}_4 \cdot 3\text{H}_2\text{O}$), 5,5'-dithiobis(2-nitrobenzoic acid) (DTNB), 4-mercaptobenzoic acid (MBA), 2,3,5,6-Tetrafluoro-4-mercaptobenzonic acid (TFMBA), thiosalicylic acid (TSA), 4-aminothiophenol (ATP), bovine serum albumin (BSA), sodium hydroxide, sodium citrate, phosphate-buffered saline (PBS, 1X), FPBS (1X PBS and 1% fetal bovine serum), trisaminomethane (Tris, 1M), 4-(2-hydroxyethyl)-1-piperazineethanesulfonic acid (HEPES, 1M), and regenerated cellulose membrane (MWCO=7000) were purchased from Sigma-Aldrich (Sydney, Australia). Distilled water (Millipore Milli-Q grade) with a resistivity of 18.2 $\text{M}\Omega \cdot \text{cm}$ was used in all the experiments. All chemicals were used as received without any purification.

Synthesis of gold nanoparticles (AuNPs)

The gold nanoparticles (AuNPs) of approximately 60nm in diameter were synthesised according to Turkevich method ¹. A solution of HAuCl_4 (0.01% w/v, 100mL) was heated to boiling under stirring at 550 rpm, followed by the addition of 0.85 mL of sodium citrate solution (1.0% w/v) in one and quick shot. The colour of the solution changed from light yellow to dark blue and after two minutes it changed to purple. The solution was boiled and stirred continuously for 20 min after the addition of sodium citrate and then was stirred without heating for 10 min. Finally, it was left to cool down to room temperature overnight protected from light. The as-prepared AuNPs were stored at 4°C.

Synthesis of BSA-templated gold nanoclusters (AuNCs)

The BSA-templated gold nanoclusters (BSA-AuNCs, or AuNCs) were synthesised according to the method developed by Xie et al ². Briefly, 5 mL of H₂AuCl₄ solution (10 mM, 37°C) was added to 5 mL of BSA solution (50 mg/mL, 37°C) under vigorous stirring for 2 min to form BSA-Au complex, which was obvious by cloudy yellow colour. Then, 0.5mL of NaOH (1 M) was added to increase the pH to alkaline condition (between 11 and 12). After incubating at 37 °C for 12 h, a clear orange-brown solution was obtained. The solution of BSA-AuNCs was thoroughly dialyzed for one day with DI water using regenerated cellulose dialysis bag (MWCO of 7000 kDa).

Conjugation of thiolated benzoic molecules to AuNPs

To prepare molecule-conjugated AuNPs (AuNPs@Mol), four thiolated benzoic molecules including MBA, TFMBA, TSA, and DTNB were used. First, AuNPs (1.5mL) suspension were centrifuged at 5500 rpm for 10 min and 500 µL of supernatant were discharged, followed by redispersion of AuNPs in 1 mL DI water. Different amounts of thiolated benzoic molecules were incubated with AuNPs (according to **Table S1** and **Figure S2**) to obtain stable molecule-coated AuNPs³. The samples were incubated at room temperature for 10 min with shaking (60 rpm, 60 degree of rotation) followed by leaving at 4°C overnight. The excess of thiolated benzoic molecules was removed by centrifugation at 5500 rpm for 10 min and the pellet was redispersed in 1.0 mL DI water.

Synthesis of AuNPs@Mol@AuNCs

To find the required amount of BSA-AuNCs that would maximise the SERS intensities of various AuNP@Mol samples used in this study, each AuNP@Mol sample was

incubated with various concentrations of BSA-AuNCs at room temperature for 90 min and the unbonded BSA-AuNCs were removed by centrifugation (5500 rpm at 4°C). To prepare AuNPs@Mol@AuNCs, 0.5 mL of AuNP@Mol were added to 0.5 mL of a mixture of BSA-AuNCs and DI water (**Table S4**). The samples were incubated for 1.5 h at room temperature followed by centrifugation at 5500 rpm for 10 min at 4°C to remove unbonded AuNCs. The pellet was redispersed in DI water to a total volume of 1.0 mL.

Statistical analysis

The statistical software GraphPad Prism version 10.1.1 for macOS, GraphPad Software, Boston, Massachusetts USA, www.graphpad.com, was used for analysis. One-Way ANOVA followed by Turkey's multiple comparisons test was implemented to determine the difference between individual groups of data.

Instrumentation

Raman spectra of the samples were collected using portable Raman microscope (IM-52, Snowy Range Instruments) at 785 nm excitation with the 15 mW laser power, integration time of 2s for four accumulations. Transmission electron microscope (TEM, Philips CM10) was used to visualise the size and morphology of the nanoparticles. The size distribution of the AuNPs, AuNP@Mol, and AuNP@Mol@AuNC were determined using Nanoparticle Tracking Analysis (NTA, Nanosight NS300). The UV-Visible spectrum of samples was recorded using a UV-Vis spectrometer (NanoDrop 2000, Thermo Scientific and Jasco V-760). Excitation and emission spectra of AuNCs were measured by Spectrofluorometer Jasco-8500. Fluorescence lifetime was measured using a FluoTime 200 TCSPC machine (Picoquant BmbH, Germany) by exciting samples at 373 nm by using a Opolette tunable laser system (≈ 5 ns pulse, 20

Hz), and obtaining emission at 605 nm. Absorption of all samples were set at 0.2 OD at excitation wavelength. Spectra at different time delays were collected at variable gate widths by using Andor iStar DH320T-18U-E3 intensified CCD (2 ns resolution), which is paired with a Kymera 193i-A spectrometer. A two exponential model was used to analyse the data and calculate the average fluorescence lifetime⁴.

Simulation of enhanced electric field

COMSOL Multiphysics software package (see www.comsol.com) was used to calculate the enhanced electric field around AuNP, AuNP@BSA and AuNP@BSA-AuNCs by solving the governing equations based on Mie theory using finite-element method (FEM). The refractive index of Au was taken from, Johnson and Christy data⁵. The surrounding environment was assumed in water ($n=1.33$). The refractive index of BSA ($n=1.602$) was taken from the study of Sano, Y.⁶ Since the BSA molecules are not in solid form when they coat on the surface of AuNPs, the refractive index for BSA layer was considered as the average between $n=1.33$ and $n=1.602$ ($n=1.466$).

A plane wave linearly polarizing along the z-axis and propagating in x-direction at wavelength of 785 nm was set as the source. The diameter of each AuNP was considered as 60 nm (TEM), the diameter of Au nanoclusters was 2 nm (TEM) and the distance between AuNC and AuNP was considered as 3.5 nm.

Density functional theory calculations

All simulations were performed using the density functional theory (DFT) implemented in the Vienna ab initio Simulation Package (VASP) code^{7,8}. The generalized gradient approximation (GGA) in the form of Perdew – Burke – Ernzerhof (PBE) treats the exchange – correlation interactions, while the frozen-core projector augmented wave

(PAW) approximation describes the interaction between the ion and electron⁹⁻¹¹. In order to incorporate the effects of nonlocal van der Waals (vdW) interactions that are not included correctly in conventional DFT calculations, the DFT-D3 method in Grimme's scheme was adopted for dispersion corrections here¹². A plane-wave basis set with the cut-off kinetic energy of 520 eV is employed to expand the smooth part of wave functions. The gamma-centered Monkhorst-pack k -mesh with a reciprocal space resolution of $2\pi \times 0.04 \text{ \AA}^{-1}$ and $2\pi \times 0.03 \text{ \AA}^{-1}$ were utilized for structural optimization and static self-consistent calculations, respectively. The $(2\sqrt{3} \times 4)$ Au (111) and Ag(111) surfaces were modelled by a 4-layer slab, separated by a vacuum layer of more than 20 Å to avoid interactions between periodic slabs, as shown in **Figure S11**. For the models with Au cluster, a $(3\sqrt{3} \times 4)$ supercell of metal surface was utilized. When geometries of all structures were optimized, the top two layers of the surfaces including adsorbate were relaxed, while the bottom two layers were fixed. The structural relaxation was performed until Hellmann–Feynman forces were less than 0.01 eV/Å and the convergence criteria of 10^{-5} eV for total energy in the self-consistent field iteration were set (**Figure S12**). In this study, five molecules including ATP, DTNB, MBA, TFMBA, and TSA, as shown in **Figure S13**, were considered for the DFT calculations to explore the charge transfer mechanism with/without Au cluster.

To simulate the Raman spectrum of the previously optimised structures for different molecules were used. The triple split valence basis set of 6-311+G was adapted. The Raman frequency calculation was performed at the same level^{13, 14}.

Table S1. Amount of thiolated benzoic molecule used in the conjugation with AuNPs.

Thiolated benzoic molecule	Volume (μL)	Concentration (mM)	Conjugation Conditions-Step 1	Conjugation Conditions-Step 2
DTNB	10	1	Incubation by shaking (60 rpm, angle of rotation: 60°) at room temperature for 10 min	Leaving at 4°C, overnight, Undisturbed
TFMBA	8	1		
MBA	5	1		
TSA	5	1		

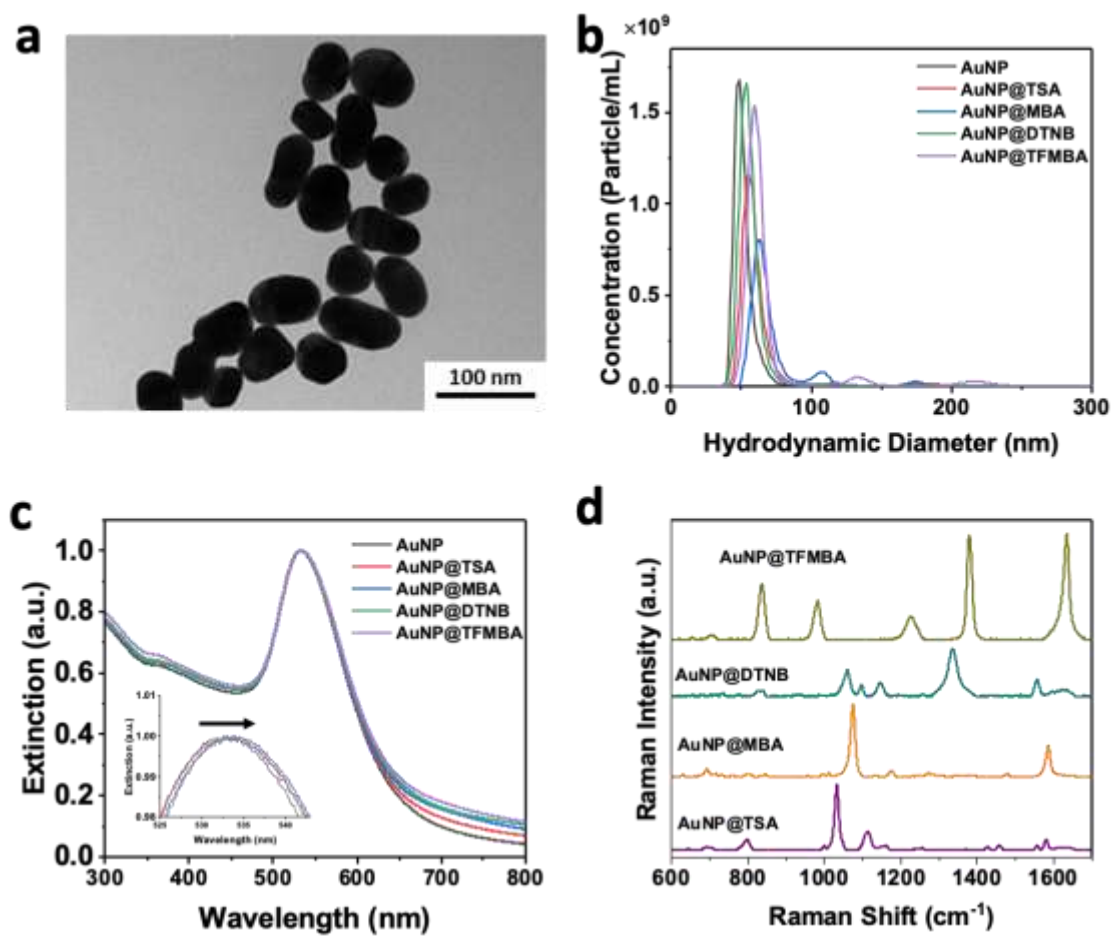


Figure S1. a) TEM of AuNPs, b) NTA of AuNP@Mol samples, c) UV-Visible spectra for AuNP and AuNP@Mol samples, insert graph: redshift in LSPR peak of AuNPs after conjugation with different molecules (AuNP@Mol); and d) Raman spectra of different AuNP@Mol samples at 785 nm excitation

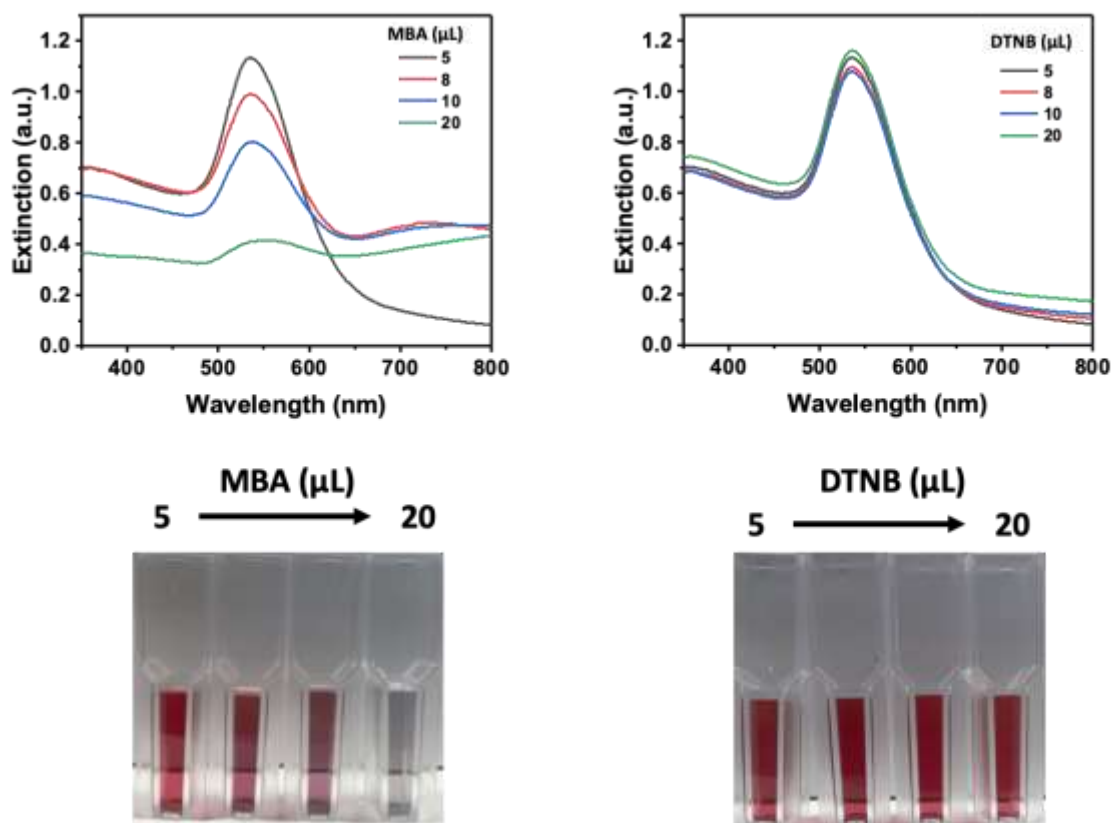


Figure S2. Left: UV-Visible spectra of AuNPs after incubation with different volumes of MBA (1 mM, Volume: 5-20 μL) in ethanol and photographs of corresponding samples, Right: UV-Visible spectra of AuNPs after incubation with different volumes of DTNB (1 mM, Volume: 5-20 μL) in ethanol and photographs of corresponding samples

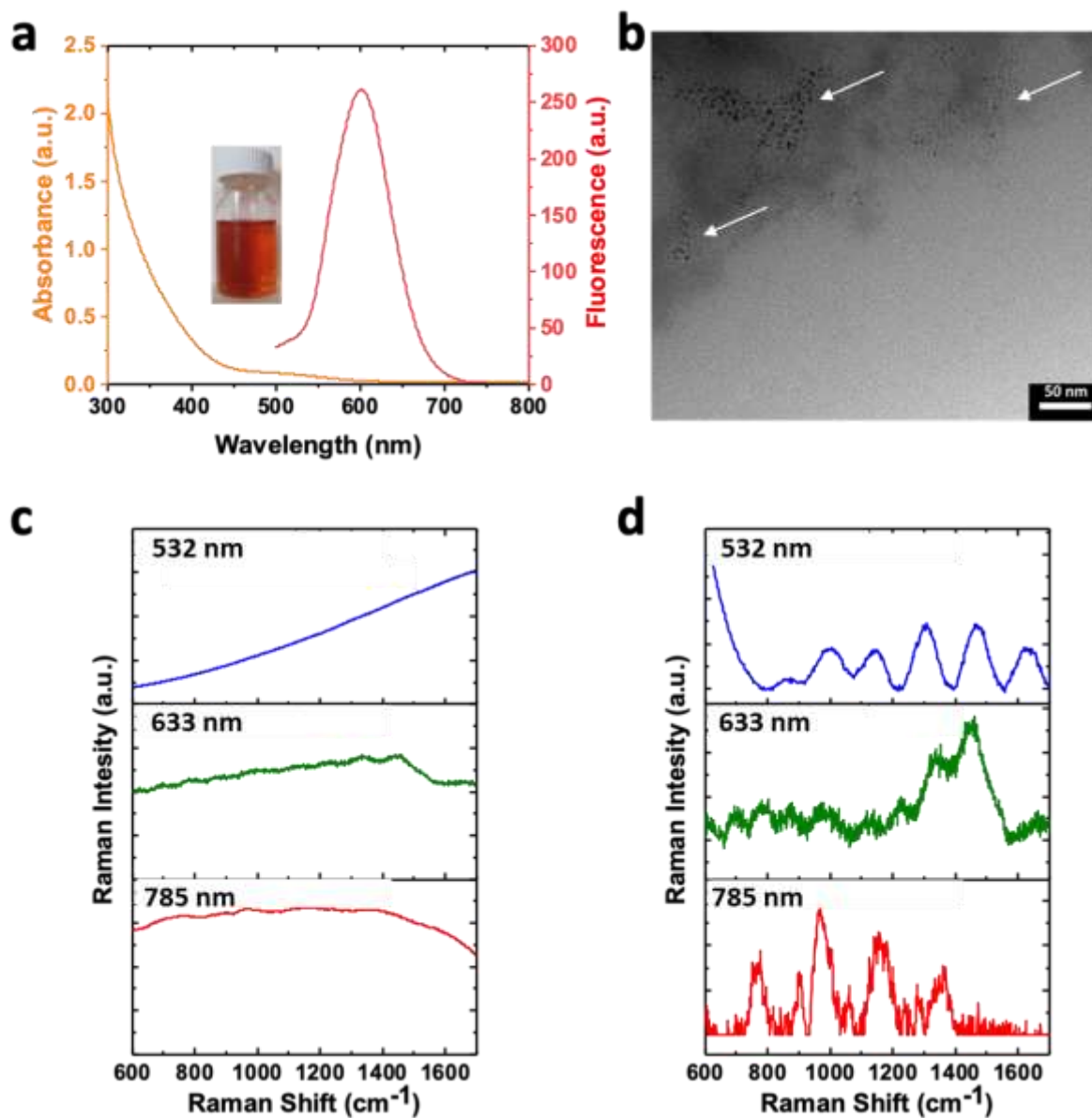


Figure S3. a) Absorbance and fluorescence spectra of BSA-templated AuNCs. Excitation wavelength was 470 nm. b) TEM image of BSA-AuNCs. Raman spectra of BSA-AuNCs under different excitation wavelengths before (c) and after (d) removing the fluorescence background

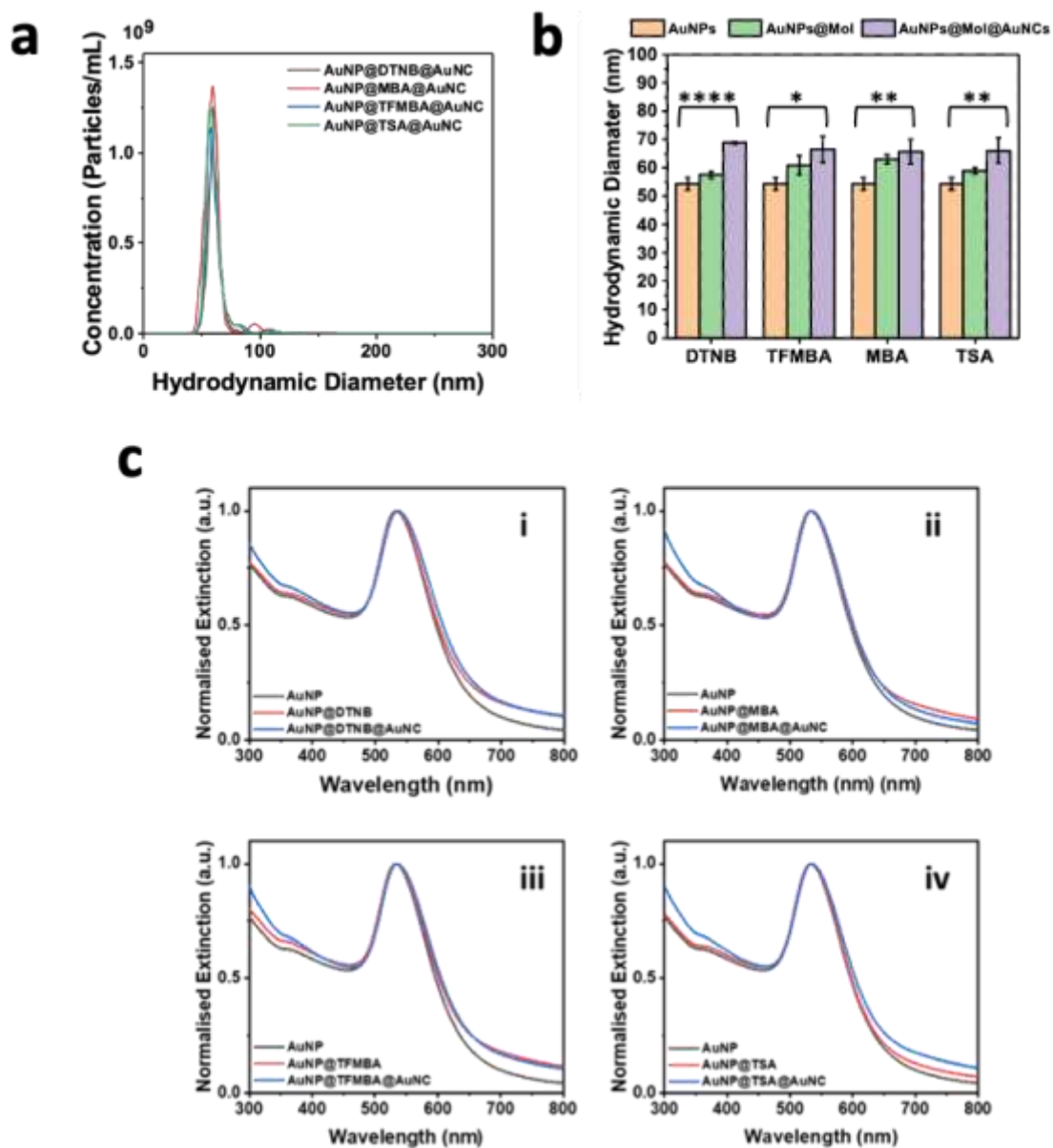
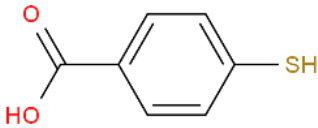
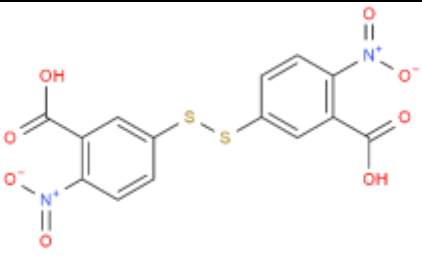
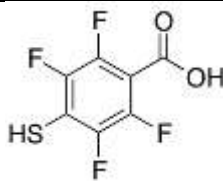
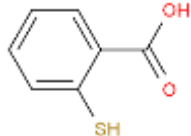


Figure S4. NTA spectra (a), statistical analysis of hydrodynamic size (b) for AuNPs, AuNPs@Mol and AuNPs@Mol@AuNCs, and UV-Visible spectra (c) of AuNP, AuNP@Mol and AuNP@Mol@AuNCs, i) Mol=DTNB, ii) Mol=MBA, iii) Mol=TFMBA, and iv) Mol=TSA. The average and standard deviation are for replicate measurements ($n = 3$). In the ANOVA: *: $p < 0.05$, **: $p < 0.01$, ***: $p < 0.001$, and ****: $p < 0.0001$.

Table S2. Assignment of Raman vibration peaks for different molecules according to literature

Raman molecule	Molecular structure	Characteristic peaks on Raman
4-mercaptobenzoic acid (MBA)		1077 cm ⁻¹ : Aromatic ring vibration C-S stretching ¹⁵ 1175 cm ⁻¹ : Aromatic C-H in-plane vibration ¹⁶ 1587 cm ⁻¹ : Aromatic C=C stretching ¹⁵
5,5'-dithiobis (2-nitrobenzoic acid) (DTNB)		1061 cm ⁻¹ : Aromatic ring vibration, C-S stretching ¹⁶ 1150 cm ⁻¹ : Aromatic C-H in-plane vibration ¹⁶ 1337 cm ⁻¹ : Symmetric nitro stretching ^{15, 16} 1557 cm ⁻¹ : Aromatic C=C stretching ¹⁶
2,3,5,6-tetrafluoro-4-mercaptobenzoic acid (TFMBA)		985 cm ⁻¹ : OH...O out of plane deformation ¹⁶ 1378 cm ⁻¹ : Ring stretch/C-F stretch ¹⁶ 1635 cm ⁻¹ : C=O stretching ¹⁶
Thiosalicylic acid (TSA)		1032 cm ⁻¹ : Aromatic ring vibration ¹⁷ , C-S stretching ¹⁶ 1118 cm ⁻¹ : C-O stretch ¹⁶ 1583 cm ⁻¹ : Aromatic C=C stretching ¹⁶

SI-1: Enhancement factor calculation.

The SERS enhancement factor was determined from the ratio of the Raman intensity of molecule-containing nanoparticles (AuNP@Mol) and Raman intensity of the molecules in the solution. For each molecule, the Raman peak that had the highest intensity was chosen for this comparison.

For Reference solution: We measure the Raman spectrum for a solution of Molecule with specific concentration (C_{Molecule}) in 0.1 M NaOH solution.

I_{Molecule} – Raman intensity of molecule at its maximum peak – read from the graph,

C_{Molecule} : Concentration of the Molecule

The volume of laser spot was used to calculate the number of molecules that are being excited by 785 nm laser. The diameter (d) of the laser spot in the liquid is 40 μm , pathlength (h) is 10 mm,

$$V_{\text{Laser spot}} = \pi \left(\frac{d}{2} \right)^2 \cdot h = \pi (20\mu\text{m})^2 \cdot 10\text{mm} = 1.26 \times 10^{-5} \text{cm}^3$$

Mole of molecules in laser spot = $C_{\text{Molecule}} \cdot V_{\text{Laser spot}}$

$$\begin{aligned} N_{\text{Molecule}} &= \text{Mole of Molecules in laser spot} \cdot \text{Avogadro's constant} \\ &= \text{Mole of Molecules in laser spot} \cdot 6.02 \times 10^{23} \end{aligned}$$

For AuNP@Mol solution: We measure the Raman spectrum for a solution of AuNP@Mol in DI-water.

$C_{\text{Nanoparticle}}$: Concentration of AuNP@Mol obtained by NTA

$$V_{\text{laser spot}} = 1.26 \times 10^{-5} \text{ cm}^3$$

Surface area of each nanoparticle (D=56 nm based on TEM data):

$$S_{\text{spherical nanoparticle}} = 4\pi r^2 = 4\pi(28 \text{ nm})^2 = 9851.744 \text{ nm}^2$$

$S_{\text{Molecule}} = 0.38 \text{ nm}^2$, topological surface area for each molecule

$$\text{No. of molecules per Nanoparticle} = \frac{S_{\text{nanoparticle}}}{S_{\text{Molecule}}}$$

$$N_{\text{nanoparticle in laser spot}} = C_{\text{nanoparticle}} \cdot V_{\text{laser spot}}$$

Number of molecules on AuNPs and in laser spot: N_{SERS}

$$= N_{\text{nanoparticle in laser spot}} \cdot \text{No. of molecules per Nanoparticle}$$

ISERS – SERS intensity of molecule-containing nanoparticles at the maximum peak of molecule – read from the graph,

$$EF(\text{AuNP@Mol}) = \frac{I_{\text{SERS}}}{I_{\text{Molecule}}} \cdot \frac{N_{\text{Molecule}}}{N_{\text{SERS}}}$$

Based on the experimental data, the following results were obtained and used for SERS EF calculation

Table SI-1. The values that used for calculation of surface-enhanced Raman scattering enhancement factors

Molecule	Concentration of molecules in Reference (M)	I_{Molecule}	N_{Molecule}	Concentration of Nanoparticles	I_{SERS}	N_{SERS}	SERS EF
MBA	0.25	12078.48	1.9×10^{15}	1.72×10^{10}	13521.44	5.62×10^9	3.78×10^5
TSA	0.25	4203.17	1.9×10^{15}	2.24×10^{10}	11.67.42	7.32×10^9	7.20×10^4
DTNB	0.1	54290.02	7.59×10^{14}	2.6×10^{10}	6158.84	8.49×10^9	1.01×10^4
TFMBA	0.35	7045.58	2.65×10^{15}	2.26×10^{10}	5173.71	7.38×10^9	2.64×10^5

Table S3. Raman peak assignment for bovine serum albumin¹⁸

Vibration (Raman shift)	Interpretation
955 cm ⁻¹	symmetric stretching vibration COOH groups
1159 cm ⁻¹	stretching vibration of C-N bond in Phe and Tyr
1550 cm ⁻¹	C-N stretching vibration of Phe and acid amides (not enhanced)

Table S4. Amount of BSA-AuNCs used in the conjugation with AuNP@Mol to prepare AuNP@Mol@AuNC

BSA-AuNCs (μL)	DI Water (μL)	AuNP@Mol (μL)
0	500	500
25	475	500
50	450	500
75	425	500
100	400	500
200	300	500
300	200	500

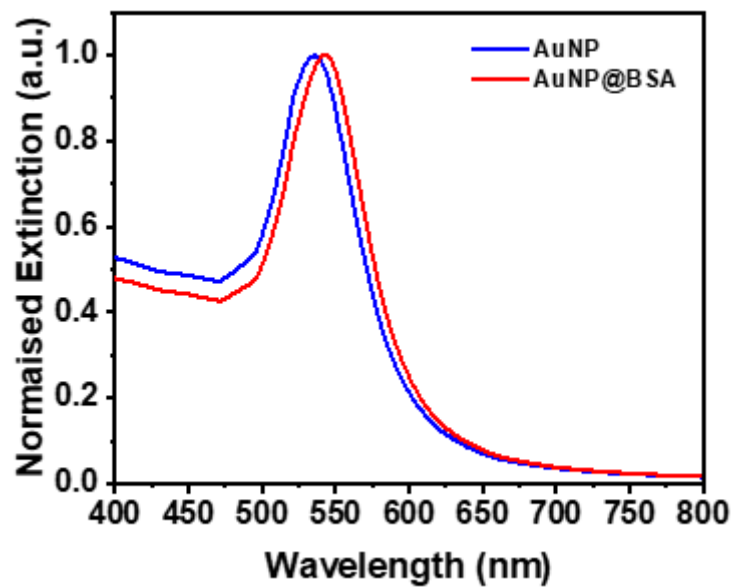


Figure S5. Simulation results for spectra of AuNP and AuNP@BSA.

Table S5. Zeta potential value for AuNP, AuNC, and different AuNP@Mol and AuNP@Mol@AuNX samples

Sample	Zeta Potential (mV)	Sample	Zeta Potential (mV)
AuNP	-32.82±2.75	AuNC	-12.6±0.86
AuNP@TSA	-30.18±0.24	AuNP@TSA@AuNC	-23.36±2.83
AuNP@TFMBA	-34.7±0.47	AuNP@TFMBA@AuNC	-30.6±2.25
AuNP@DTNB	-31.18±0.25	AuNP@DTNB@AuNC	-24.56±2.35
AuNP@MBA	-31.68±0.62	AuNP@MBA@AuNC	-24.86±4.43
AuNP@ATP	-25.4±2.18	AuNP@ATP@AuNC	-23.1±0.77

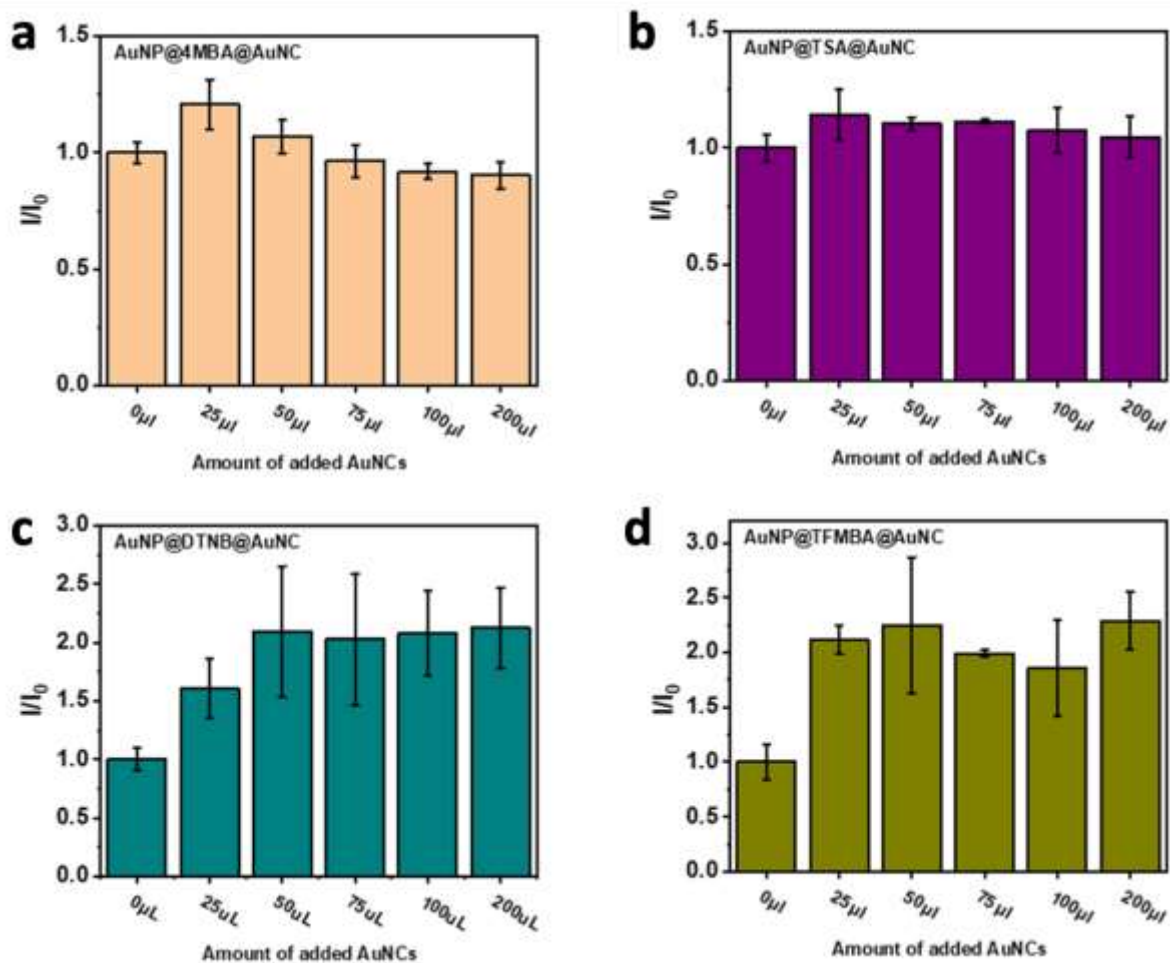


Figure S6. AuNP@Mol@AuNC SERS signals compared with control (0 μ L of AuNC refers to AuNP@Mol samples). a) AuNP@MBA@AuNC. b) AuNP@TSA@AuNC. c) AuNP@DTNB@AuNC. d) AuNP@TFMBA@AuNC. The average and standard deviation are for replicate measurements ($n = 3$).

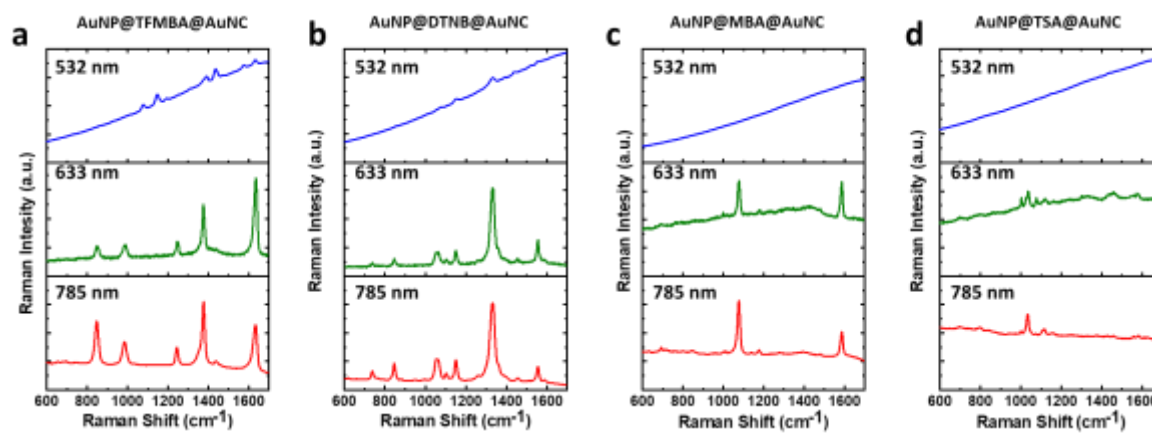


Figure S7. Raw data for wavelength-dependent SERS spectra of different AuNP@Mol@AuNC samples: a) TFMBA, b) DTNB, c) MBA, and d) TSA.

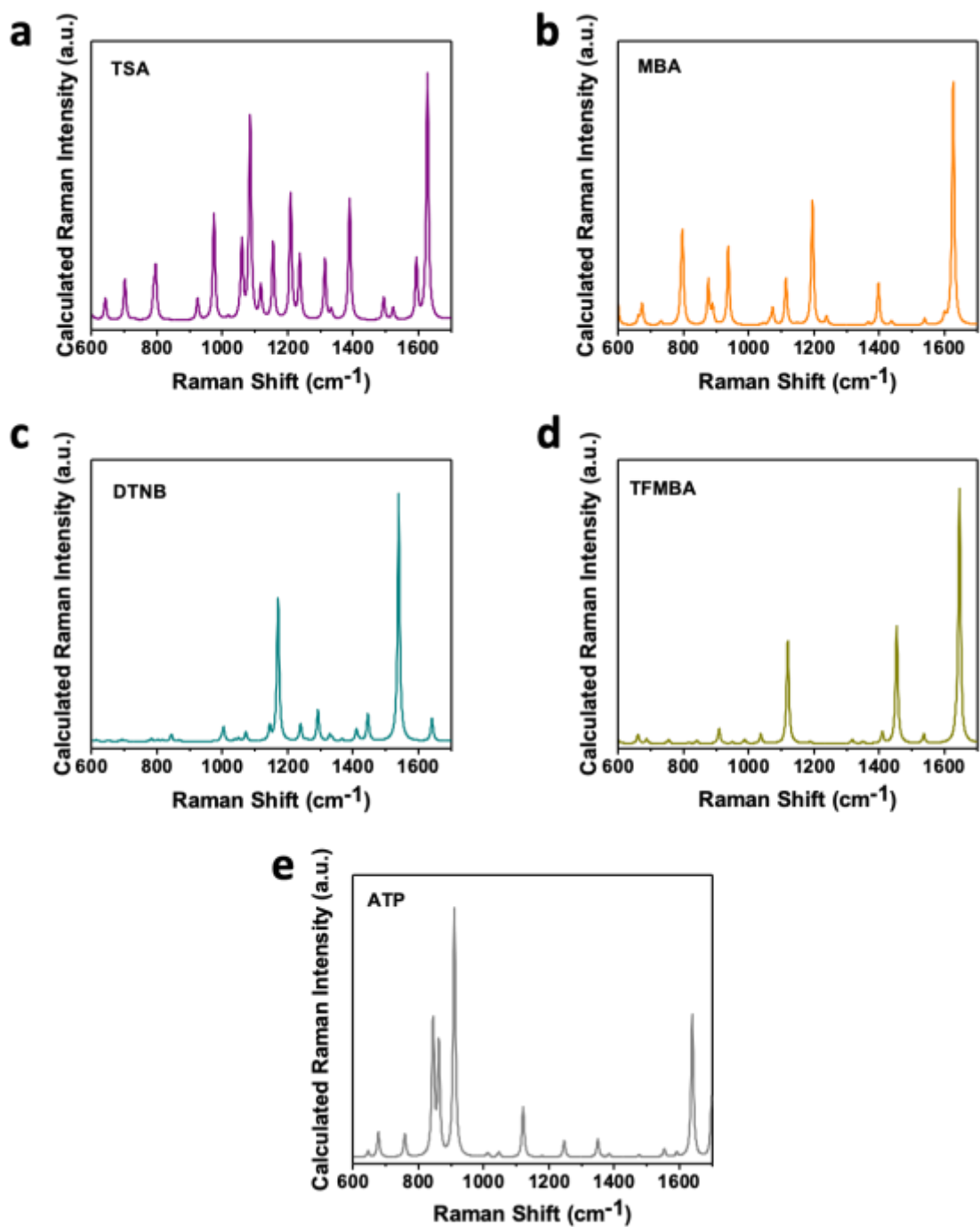


Figure S8. Simulated Raman spectra for different molecules: a) TSA, b) MBA, c) DTNB, d) TFMBA, and e) ATP.

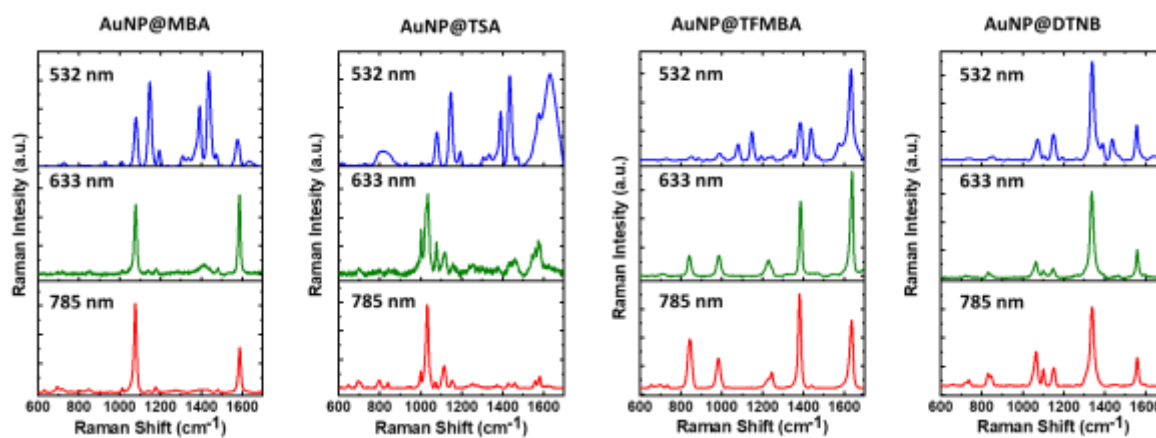


Figure S9. Wavelength-dependent SERS spectra of different AuNP@Mol samples: a) MBA, b) TSA, c) TFMBA, and d) DTNB.

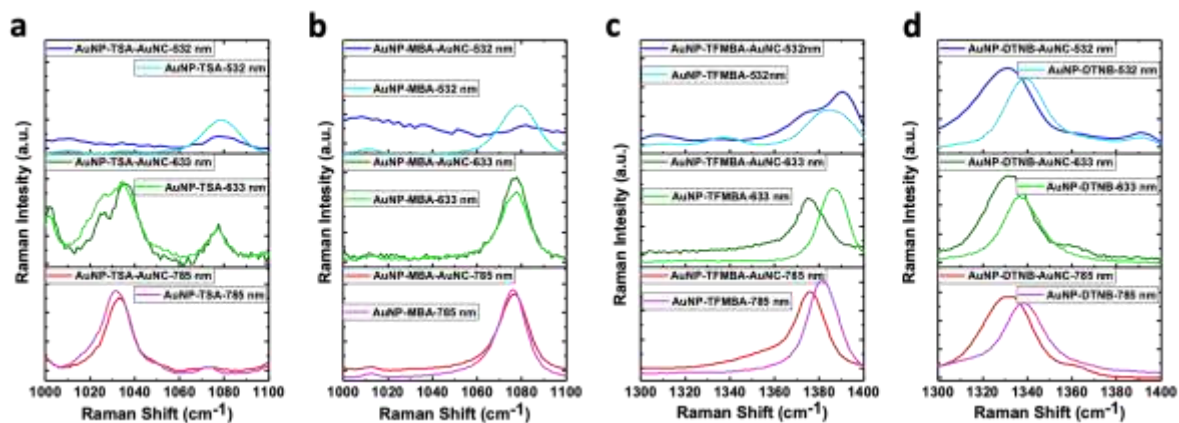


Figure S10. Comparison between the peak position for the dominant SERS peak in different samples (AuNP@Mol and AuNP@Mol@AuNC) and under different Raman excitation wavelengths: a) MBA, b) TSA, c) TFMBA, and d) DTNB.

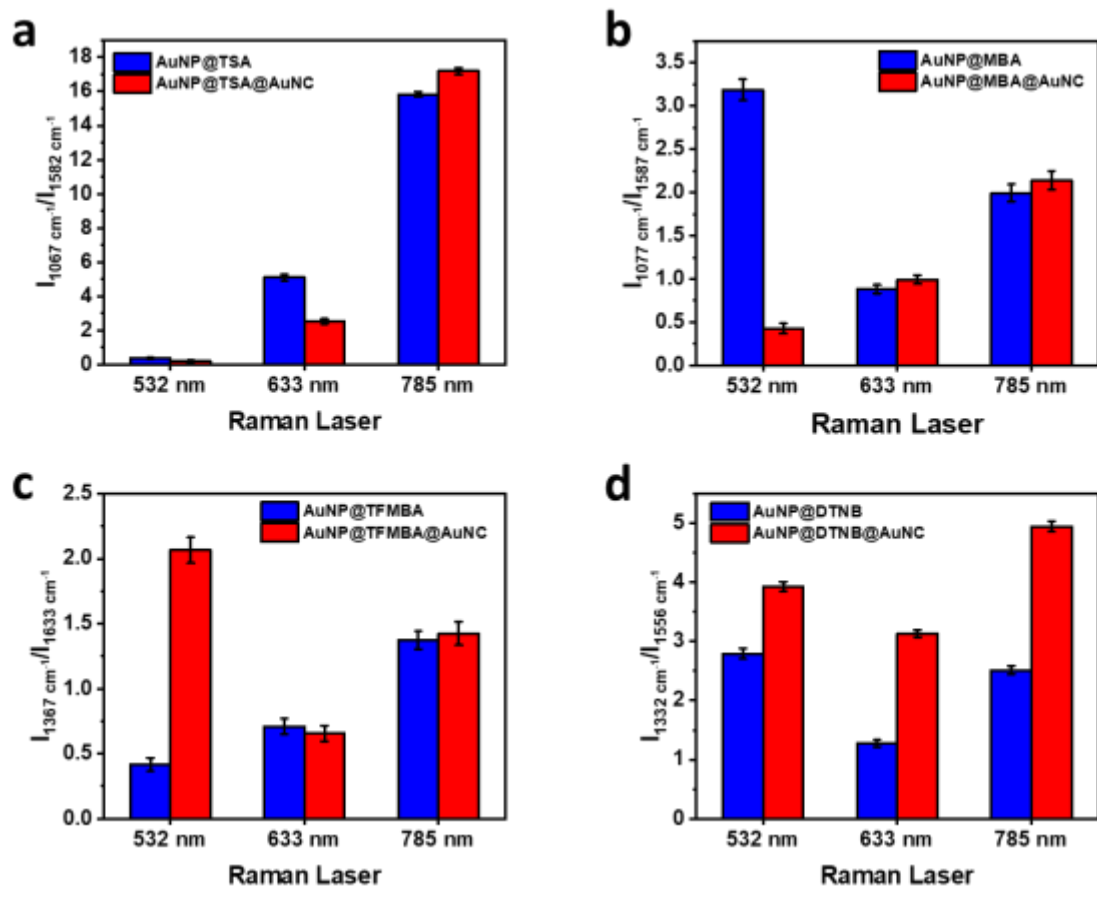


Figure S11. The ratio between the two main peaks in SERS spectra in AuNP@Mol and AuNP@Mol@AuNC: a) MBA, b) TSA, c) TFMBA, and d) DTNB. The average and standard deviation are for replicate measurements (n = 3).

Table S6. Assignment of Raman peaks for different molecules using DFT calculation

Molecule	Raman Shift (cm ⁻¹)	Peak Assignment
ATP	637	CCC deformation in-plane
	701	C-H vibration out-of-plane
	804	C-H vibration out of plane
	1004	CCC deformation in-plane
	1078	C-S stretching vibration
	1177	C-H in-plane
	1392	C-N stretching vibration
	1423	C-H vibration, C-N bending
	1486	CCH deformation bend
	1582	Symmetric NH ₂ bending
MBA	1077	Ring breathing and C-S vibration
	1177	COOH and C-C between the ring and COOH
	1387	COOH deformation
	1586	CCC stretching vibration mode
TSA	693	CCC deformation (in-plane)
	790	C-C (ring and ring+COOH) vibration (out pf plane)
	999	C-H vibration (out pf plane)
	1033	S-H vibration, C-S stretching
	1067	C-H vibration (out pf plane)
	1115	Ring breathing
	1151	COOH and C-S
	1425	C-H vibration, symmetric, in plane
	1458	C-H vibration, asymmetric, in plane
	1558	C-H shear vibration mode, in plane
1582	C-H shear vibration mode, in plane	
TFMBA	847	SH vibration, in plane
	985	OH...O out of plane deformation
	1244	CCC Ring deformation and COOH, in plane
	1376	Ring breathing /C-F stretching
	1633	C=O stretching
	1438	CCC Ring deformation, in plane
	1077	C-S stretching
	1147	CCC ring deformation and S-H vibration
	1193	CCC Ring deformation
	1573	CCC Ring deformation
DTNB	737	vibration of nitro group
	846	OH in COOH (out of plane)
	1060	C-H in ring, out of plane
	1103	C-N stretching
	1150	C-S stretching
	1332	Symmetric nitro stretching
	1456	C-H in CH ₂ scissoring
	1556	C=C deformation, in plane

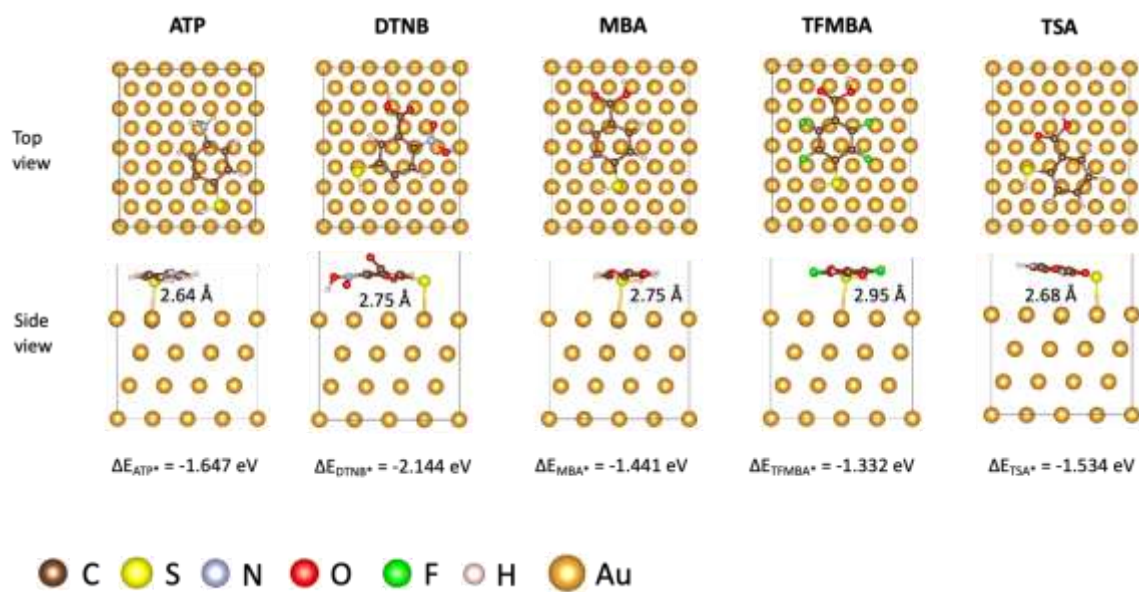


Figure S12. The optimised structures for Au(111)@Mol.

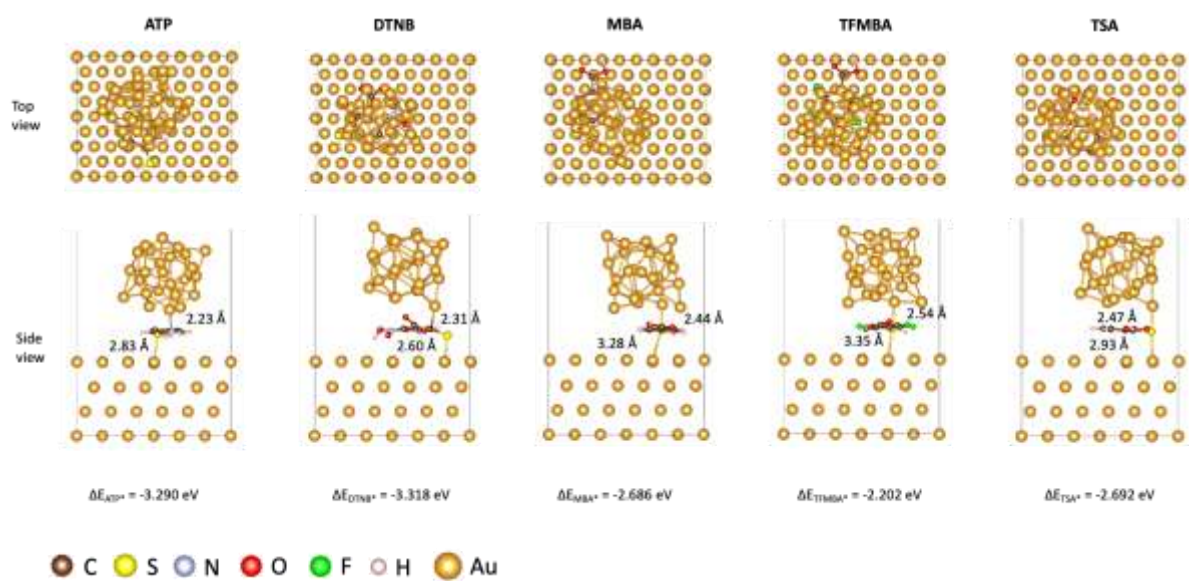


Figure S13. The optimized structures for Au(111)@Mol@Au₂₅ nanocluster.

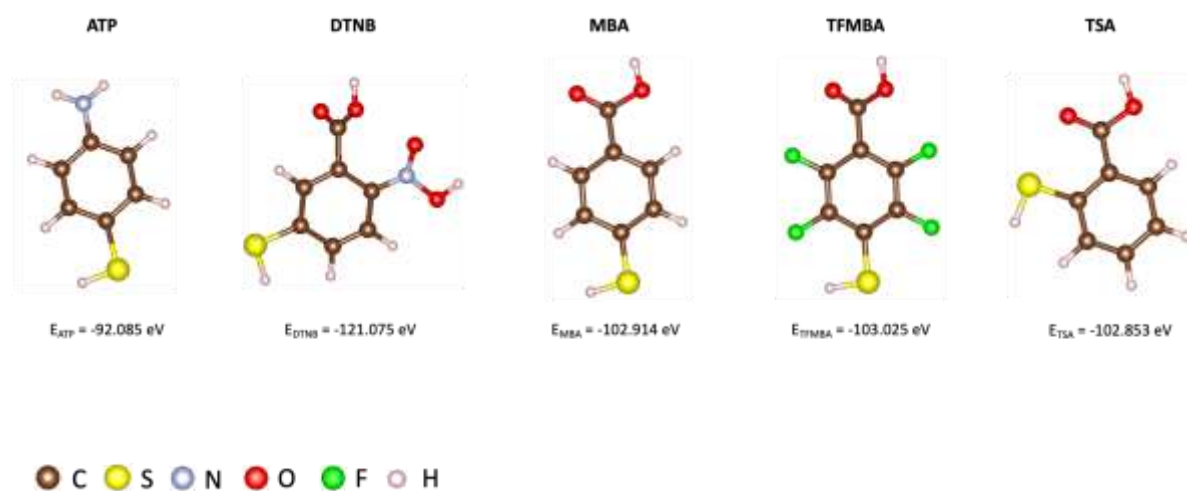


Figure S14. Structures of different molecules and the corresponding calculated optimised energy level.

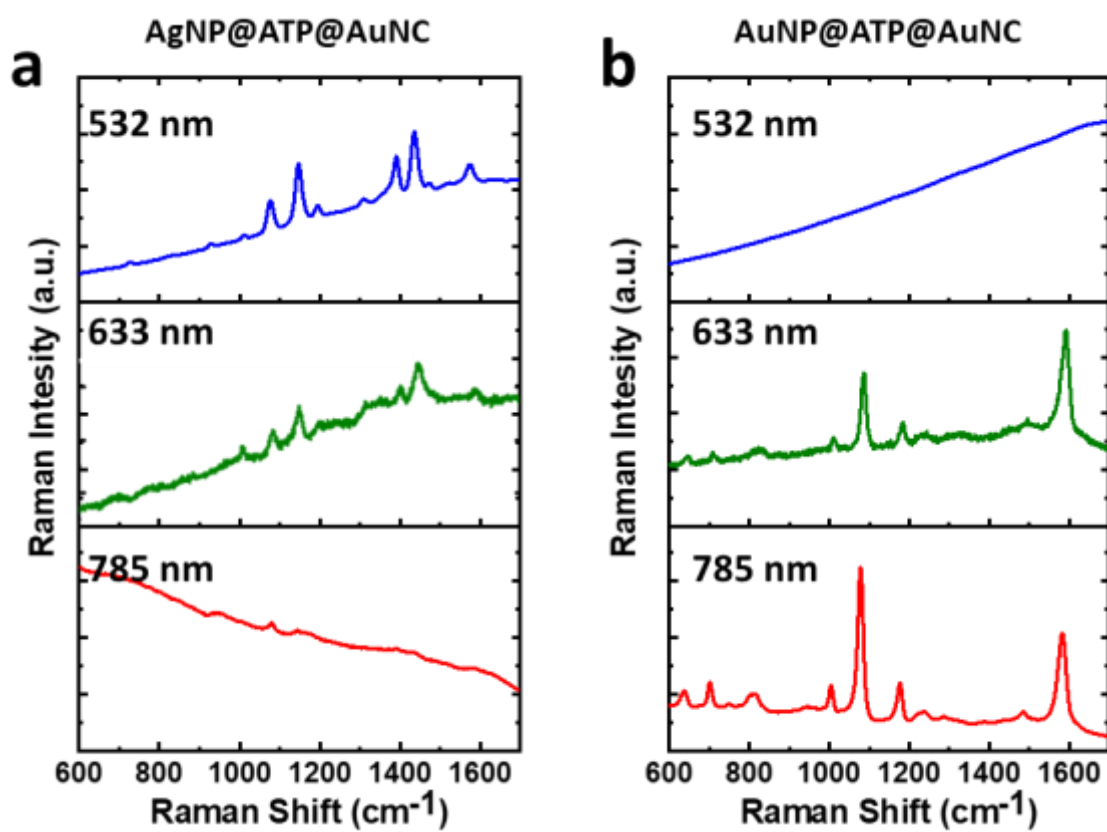


Figure S15. Raw data for wavelength-dependent SERS spectra of a) AgNP@ATP-AuNC and b) AuNP@ATP-AuNC.

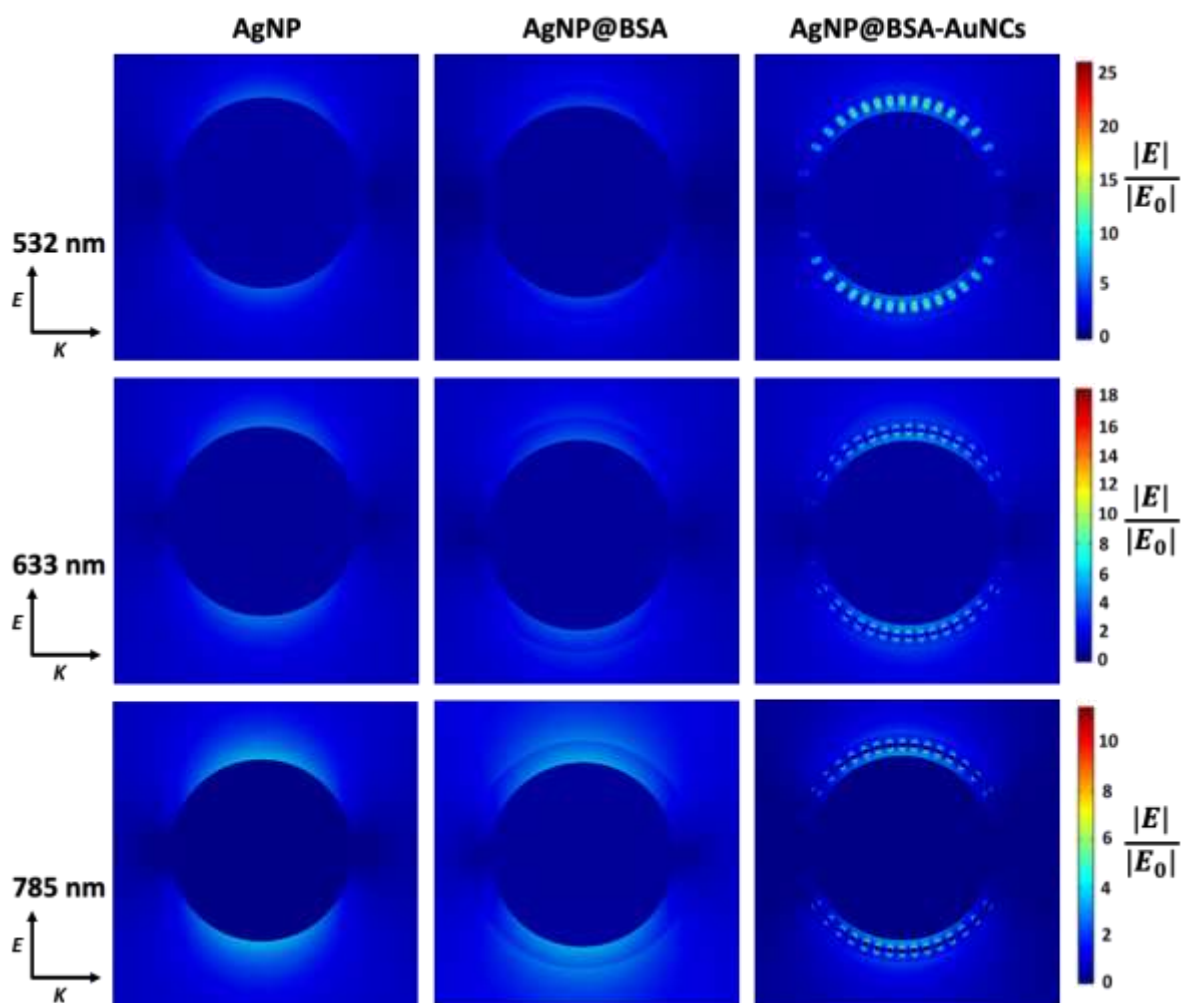


Figure S16. Simulated enhanced electric field ($\frac{|E|}{|E_0|}$) distribution around AgNP, AgNP@BSA and AgNP@BSA-AuNCs under incident light with different wavelengths (532 nm, 633 nm, and 785 nm). E indicates the polarization direction and K indicates the propagation direction of light. The diameter of AuNP was 50 nm and diameter of AuNCs was 2 nm.

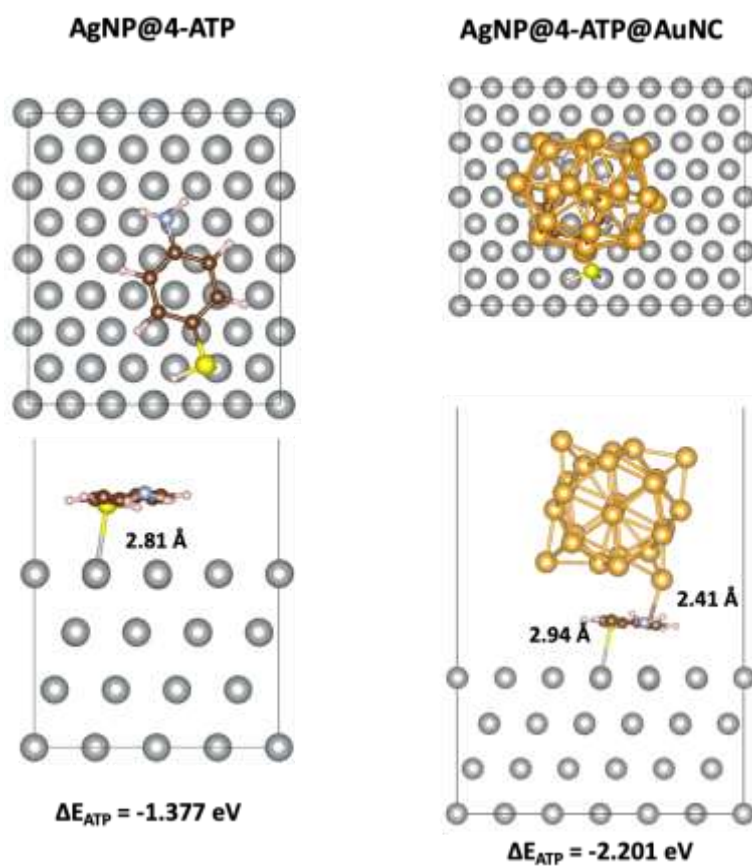


Figure S17. The optimised structures for Ag(111)@4-ATP@Au₂₅ nanocluster.

References

1. J. Turkevich, P. C. Stevenson and J. Hillier, *Discussions of the Faraday Society*, 1951, **11**, 55-75.
2. J. Xie, Y. Zheng and J. Y. Ying, *Journal of the American Chemical Society*, 2009, **131**, 888-889.
3. E. Stepula, X.-P. Wang, S. Srivastav, M. König, J. Levermann, S. Kasimir-Bauer and S. Schlücker, *ACS Applied Materials & Interfaces*, 2020, **12**, 32321-32327.
4. M. Y. Berezin and S. Achilefu, *Chemical Reviews*, 2010, **110**, 2641-2684.
5. P. B. Johnson and R. W. Christy, *Physical Review B*, 1972, **6**, 4370-4379.
6. Y. Sano, *Journal of Colloid and Interface Science*, 1988, **124**, 403-406.
7. G. Kresse and J. Furthmüller, *Physical Review B*, 1996, **54**, 11169-11186.
8. G. Kresse and J. Furthmüller, *Computational Materials Science*, 1996, **6**, 15-50.
9. P. E. Blöchl, *Physical review B*, 1994, **50**, 17953.
10. G. Kresse and D. Joubert, *Physical review b*, 1999, **59**, 1758.
11. J. P. Perdew, K. Burke and M. Ernzerhof, *Physical review letters*, 1996, **77**, 3865.
12. S. Grimme, *Journal of computational chemistry*, 2006, **27**, 1787-1799.
13. R. Krishnan, J. S. Binkley, R. Seeger and J. A. Pople, *The Journal of Chemical Physics*, 1980, **72**, 650-654.
14. R. C. Binning Jr. and L. A. Curtiss, *Journal of Computational Chemistry*, 1990, **11**, 1206-1216.
15. A. Kaminska, K. Winkler, A. Kowalska, E. Witkowska, T. Szymborski, A. Janeczek and J. Waluk, *Sci Rep*, 2017, **7**, 10656.
16. G. Socrates, *Infrared and Raman characteristic group frequencies: tables and charts*, John Wiley & Sons Ltd, Third edn., 2001.
17. Y. Hong, R. Wang, Z. Jiang, Z. Cong and H. Song, *Int J Anal Chem*, 2020, **2020**, 9271236.
18. W. Xiaodan, Z. Dawei, Z. Ping, L. Taifeng, W. Huiqin and Z. Yongwei, *Journal of Applied Biomaterials & Functional Materials*, 2018, **16**, 157-162.